J. Fluid Mech. (1985), *vol.* 155, *pp.* 267–287
Printed in Great Britain

Solutions and stability criteria of natural convective flow in an inclined porous layer

By J. P. CALTAGIRONE

Laboratoire d'Energétique et Phénomènes de Transfert, Unité Associée CNRS n° 873,
Ecole Nationale d'Arts et Métiers, Esplanade des Arts et Métiers,
33405 TALENCE CEDEX (France)

AND S. BORIES

Institut de Mécanique des Fluides de Toulouse, Laboratoire associé CNRS n° 5,
E.N.S.E.E.I.H.T., 2 rue Charles Camichel,
31071 TOULOUSE CEDEX (France)

(Received 27 March 1984 and in revised form 4 December 1984)

Previous experiments on natural convection in a differentially heated porous layer with large lateral dimensions gave evidence for different configurations of flow. Depending on the values of the Rayleigh number, the inclination and the longitudinal extension of the layer, the three main structures observed correspond to a two-dimensional unicellular flow, polyhedral convective cells and longitudinal coils. In this paper there is a definition of the conditions necessary for these types of flow to exist using a linear stability theory and it is shown that the experimentally observed structures can be theoretically predicted by a three-dimensional numerical model based upon Galerkin's spectral method. Finally, the results of this model are used to show the influence of initial conditions on the setting up of the stationary flow.

1. Introduction

When an inclined porous layer saturated by a fluid satisfying the Boussinesq approximation is differentially heated, a wide range of two-dimensional, three-dimensional, stationary or non-stationary flow configurations appear. These configurations depend on the geometric dimensions of the porous media (aspect ratio $A = L/H$, $B = M/H$, with L the length, M the width and H the thickness), on the angle of inclination ϕ and on the filtration Rayleigh number Ra^*.

As has been observed by Bories & Combarnous (1973), these flows respectively form:

(i) polyhedral cells with a vertical axis when the inclination is between 0° and 15° approximately;

(ii) longitudinal rolls, facing towards the greatest slope superimposed onto the basic unicellular flow, for ϕ varying between 15° and ϕ_c such that $Ra^* \cos \phi_c = 4\pi^2$;

(iii) a single two-dimensional cell (basic flow) which is maintained for angles greater than 90°, when $\phi > \phi_c$;

(iv) an unsteady oscillating flow which is characterized by longitudinal rolls oscillating along their axis when the layer is inclined and the $Ra^* \cos \phi$ product is greater than about 250;

(v) a clearly fluctuating flow for large values of the Rayleigh number. For a horizontal porous layer, this flow has been largely studied by Caltagirone (1975), Horne (1979), Schubert & Straus (1979), and Horne & Caltagirone (1980).

When the inclined angle is lower than, but close to, 15° hysteresis effects associated with various flow structures for given values of Ra^*, ϕ, A and B have been established by Bories, Combarnous & Jaffrennou (1972).

During the last ten years, several authors have endeavoured to deduce the criterion for transition between the different configurations of such flows. Jaffrennou and Bories (1974) determined the transition conditions between unicellular flow and flow with longitudinal coils, for a finite-extension layer, from a semi-empirical method based on a mean longitudinal thermal gradient deduced from the experiment. In 1975, Weber demonstrated that a three-dimensional perturbation is steadier than a two-dimensional one if ϕ is close to zero. In 1980, in a study devoted to the analysis of the convection in slightly inclined porous layers, Walch & Dulieu put forward solutions corresponding to reverse unicellular flow for angle values of less than 7°. The existence of different flow configurations and the transition between them was also investigated by means of two- and three-dimensional numerical simulations (Chan, Ivey & Barry 1970; Walch 1980; Caltagirone & Bories 1980) using Galerkin's spectral method or finite-difference methods.

Despite the rather numerous works on the study of convective motions in an inclined porous layer, the results obtained are still very scattered and require completion in many areas. Three of them will be studied in particular in this paper:

(i) transition between the flows in polyhedral cells and in longitudinal coils;

(ii) transition between the unicellular flow and the longitudinal-coils flow for finite parameters of the porous layer;

(iii) numerical simulation of the three-dimensional flows in cavities whose parameters A and B are close to those corresponding to the experimental observations.

2. Statement of the problem

Let us consider a porous layer of height H, where lateral dimensions L and M define the two parameters $A = L/H$ and $B = M/L$. This layer, which is inclined at an angle ϕ with respect to the horizontal line and is composed of a solid substratum of porosity ϵ, permeability K and heat capacity $(\rho c)_s$, is saturated by a fluid of thermal expansion coefficient β, of viscosity ν, heat capacity $(\rho c)_f$ and density ρ as a linear function of temperature. The porous media thus created has an apparent thermal conductivity λ^* and a heat capacity $(\rho c)^* = \epsilon(\rho c)_f + (1-\epsilon)(\rho c)_s$ (Combarnous & Bories 1975).

According to the Boussinesq approximation, the equations to which the phenomena are subject can be written in a non-dimensional form:

$$\nabla \cdot \boldsymbol{V} = 0; \tag{1}$$

$$-\nabla p + Ra^* \boldsymbol{k} T - \boldsymbol{V} = 0; \tag{2}$$

$$\frac{\partial T}{\partial t} - \nabla^2 T + \boldsymbol{V} \cdot \nabla T = 0; \tag{3}$$

where $\boldsymbol{k} = \sin\phi\, \boldsymbol{e}_1 + \cos\phi\, \boldsymbol{e}_3$ stands for the unit gravitational acceleration vector, $\boldsymbol{V} = U\boldsymbol{e}_1 + V\boldsymbol{e}_2 + W\boldsymbol{e}_3$ is the filtration velocity vector and $Ra^* = g\beta\, \Delta T K H (\rho c)_f / \nu \lambda^*$ is the filtration Rayleigh number.

The parallel surfaces containing the layers of height H are impermeable and isothermal, the lateral ones impermeable and insulating. The geometric configuration and boundary conditions are shown in figure 1.

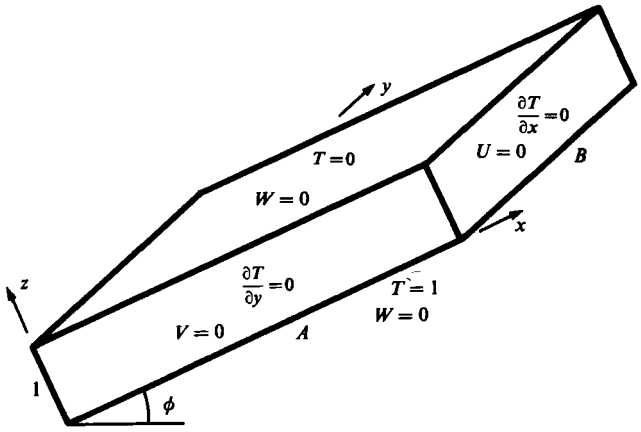

FIGURE 1. The porous layer.

3. Establishment of transition criteria

The basic flow which develops in a differentially heated inclined porous layer is of a unicellular two-dimensional type. The structure of this flow as well as its stability are defined not only by the slope angle ϕ and the Rayleigh number Ra^*, but also by the parameters A and B. In order to make comparison with the experimental results previously observed, the stability analysis will be respectively developed for $A, B \to \infty$ and A and B remaining finite.

3.1. *Stability of the flow in an infinite-extension layer*

If the porous layer is of infinite extension in the x- and y-directions, the solution corresponding to the basic unicellular flow can be readily found and leads to the following expressions for the temperature and velocity fields:

$$T_0 = 1-z; \quad U_0 = Ra^* \sin\phi\,(\tfrac{1}{2}-z); \quad V_0 = 0; \quad W_0 = 0. \tag{4}$$

Equations of perturbation relative to this flow, deduced from the (1), (2), (3) system become:

$$\nabla^2\theta - Ra^* \sin\phi\,(\tfrac{1}{2}-z)\frac{\partial\theta}{\partial x} + w = \frac{\partial\theta}{\partial t}; \tag{5}$$

$$\nabla^2 w + Ra^*\left[\sin\phi\,\frac{\partial^2\theta}{\partial x\,\partial z} - \cos\phi\left(\frac{\partial^2\theta}{\partial x^2}+\frac{\partial^2\theta}{\partial y^2}\right)\right] = 0; \tag{6}$$

where θ and w stand for the perturbations of the temperature and the vertical component of the filtration velocity superimposed on the basic flow (4).

Developing these perturbations into complex exponential functions of the spatial coordinates x, y and of time t and eliminating w in (5) and (6), the previous set of equations is reduced to one equation in θ:

$$(\mathrm{D}^2-s^2)^2\,\theta - \sigma(\mathrm{D}^2-s^2)\,\theta - Ra^*\cos\phi\; s^2\theta - \mathrm{i}s_x\, Ra^*\sin\phi\,[(\tfrac{1}{2}-z)(\mathrm{D}^2-s^2)\,\theta - \mathrm{D}\theta] = 0, \tag{7}$$

in which s_x represents the component of the wavenumber $s = (s_x^2+s_y^2)^{\frac{1}{2}}$ of the perturbation in the direction of the slope, and $\mathrm{D} = \mathrm{d}/\mathrm{d}z$.

The principle of stability exchange having been satisfied for the problem in

consideration, the marginal stability is then defined by $\sigma = 0$ and the problem of eigenvalues (7) can be solved by means of the Galerkin method, developing θ in the following form:

$$\theta = \sum_{k=1}^{N} a_k \sin(k\pi z).$$

By substitution, (7) can be written in the form:

$$\sum_{k=1}^{N} \left\{ \left[Ra^* \cos\phi - \frac{(l^2\pi^2+s^2)^2}{s^2} \right] \delta_{lk} - \mathrm{i}\, Ra^* \sin\phi \frac{s_x}{s^2} \frac{4lk}{(l^2-k^2)^2} \left(\frac{2s^2}{\pi^2} + l^2 + k^2 \right) \delta_{l+k,2p-1} \right\} a_k = 0, \quad (8)$$

say $\mathbb{L}(a_k) = 0$, giving a homogeneous linear system only accepting a non-zero solution for a particular value of Ra^* such that $\det \mathbb{L} = 0$.

Although the research on these values, and more particularly on the critical ones, has been done by solving (8) numerically up to the rank $N = 10$ useful information can be drawn by considering the approximation to rank $N = 2$. Indeed, if we take $s \simeq \pi$, for this rank of approximation, (8) becomes:

$$(Ra^* \cos\phi - 4\pi^2)(Ra^* \cos\phi - 25\pi^2) + Ra^{*2} \sin^2\phi \frac{s_x^2}{\pi^4} \frac{3136}{81} = 0. \quad (9)$$

So, when ϕ tends to zero,

$$Ra^* \cos\phi \simeq 4\pi^2 + 3s_x^2 \tan^2\phi. \quad (10)$$

This relation, which gives an instability condition of the basic solution (T_0, V_0) shows immediately that the longitudinal coils ($s_x = 0$) are more stable than the transversal ones or the polyhedral cells ($s_x \neq 0$). Moreover, from work on the solution of (9), as a function of the slope, it can be seen that this equation will no longer give a real solution beyond a critical angle value say ϕ_t. This result, the main consequence of which is to exclude solutions other than $s_x = 0$ beyond a certain value of the slope, is in agreement with the experimental observations confirming the presence of the single longitudinal coils within a given range of the ϕ variation.

At the rank N, the real solutions of the equation $\det \mathbb{L} = 0$ are all included between

$$Ra_1^* = \frac{(\pi^2+s^2)^2}{s^2} \quad \text{and} \quad Ra_2^* = \frac{(N^2\pi^2+s^2)^2}{s^2}$$

for $\phi = 0$. When ϕ increases, Ra_1^* tends to infinity and the function Ra_1^* is asymptotic to the value $\phi = \phi_t$. The critical value of the transition coincides with the minimum value of Ra_1^* as a function of s, that is to say:

$$Ra_c^*(\phi) = \min_s Ra_1^*(\phi).$$

Further work on this, after theoretical computation, leads to the results for the wavenumber and the critical Rayleigh number given in table 1, for the approximations $N = 5$ and $N = 8$ and with

$$Ra_L^* = \frac{Ra_c^*}{\pi} \quad \text{and} \quad s_L = \frac{s_c}{\pi}.$$

The limiting angle ϕ_t for which the solution corresponding to transverse rolls $s = s_x \neq 0$ no longer exists, is found to be equal to $\phi_t = 31° 48'$ for the approximation $N = 8$.

According to experimental observations, the analysis of three-dimensional linear

ϕ	s_L	Ra_L^* $(N = 5)$	Ra_L^* $(N = 8)$
0	1	4	4
5	0.998	4.0232	4.0232
10	0.993	4.0976	4.0976
15	0.984	4.2401	4.2402
20	0.965	4.4938	4.4940
25	0.94	4.9818	4.9820
30	0.88	6.3675	6.3680

TABLE 1

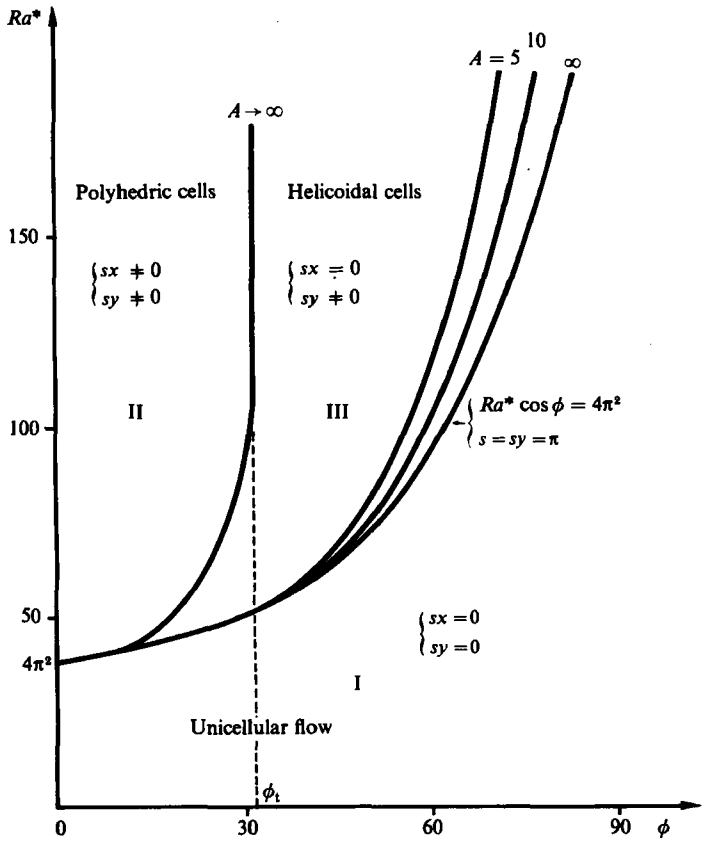

FIGURE 2. Criteria for transition between the different types of flow.

stability enables three flow domains to be distinguished in the (Ra^*, ϕ)-plane (see figure 2):

(i) for Ra^* and ϕ such that $Ra^* \cos\phi < 4\pi^2$ only the basic two-dimensional unicellular flow T_0, U_0 remains;

(ii) when the Ra^*, ϕ couple is such that $Ra^* \cos\phi > 4\pi^2$, the $s \neq 0$ three-dimensional flow becomes steady, and the $Ra^* \cos\phi = 4\pi^2$ condition, previously found by Bories & Monferran (1972), corresponding to the appearance of a flow in longitudinal coils, is confirmed well by the analysis taking $s_x = 0$;

(iii) taking Ra^* and ϕ giving representative points located over the transition defined by (8), the flow can be steady with transverse rolls $s = s_x \neq 0$ and, more

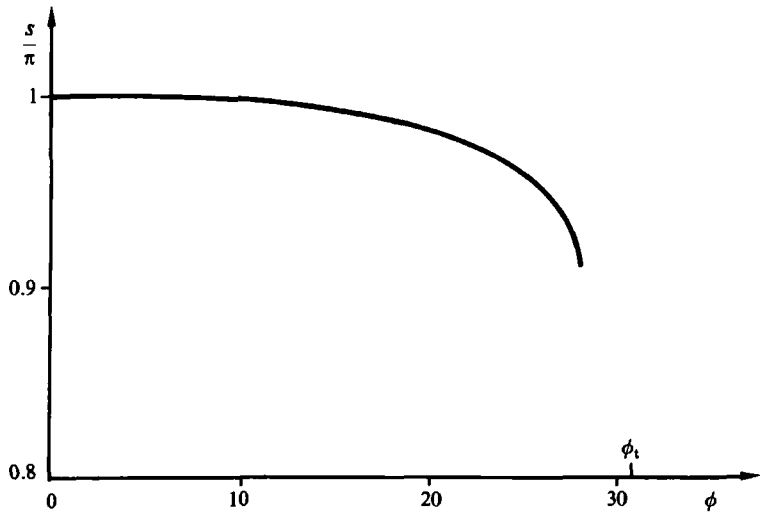

FIGURE 3. Wavenumber of the perturbation as function of the slope.

generally, with polyhedral cells $s = (s_x^2 + s_y^2)^{\frac{1}{2}}$ with $s_x \neq 0$ and $s_y \neq 0$, corresponding to the superimposition of several groups of rolls.

When the angle ϕ increases, at a fixed Ra^*, the transition between polyhedral cells or transverse and longitudinal rolls is illustrated in figure 3, showing the stretching of the cells (decrease of the wavenumber component along the Ox direction as a function of the inclination).

3.2. *Flow stability in a layer of finite extension A*

According to the modifications introduced to the basic flow by the variations of the lateral dimension A, the stability criterion $Ra^* \cos\phi = 4\pi^2$ is no longer satisfied when the extension of the layer in the direction of the inclination takes finite values. In order to determine the influence of this parameter upon the stability of unicellular flow, it is first necessary to determine the new field T_0, V_0 to be introduced into the perturbation equations. Noting that, in this case, V_0 has two components which are not zero, say: $V_0 = U_0 e_1 + W_0 e_3$, this has been determined from (1)–(3) using the Galerkin method described in §4.

Restricting the approximation rank to $N = 2$, the solution of the basic flow can be written as follows:

$$T_0 = (1-z) + a_{02} \sin 2\pi z + a_{11} \cos \pi x \sin \pi z; \tag{11}$$

$$U_0 = -Ra^* \pi^2 A^2 b_{11} \sin \pi x \cos \pi z; \tag{12}$$

$$W_0 = Ra^* \pi^2 b_{11} \cos \pi x \sin \pi z; \tag{13}$$

where the coefficients depending on the (Ra^*, ϕ) couple can be written as follows:

$$\left.\begin{aligned} a_{02} &= -\tfrac{1}{8} Ra^* \pi a_{11} b_{11}; \\ a_{11} &= Ra^* b_{11} \frac{1 + a_{02}\pi}{1/A^2 + 1}; \\ b_{11} \pi^2 (1 + A^2) &= \cos\phi \, a_{11} - \frac{16A \sin\phi}{\pi^3} (1 + \tfrac{2}{3}\pi a_{02}). \end{aligned}\right\} \tag{14}$$

Hence, we have:

$$\frac{a_{02}}{1+a_{02}\pi} = -\frac{1}{8\pi^3}\left(1+\frac{1}{A^2}\right)\left[\frac{16A\,Ra^*\sin\phi\left(\frac{1}{\pi}+\frac{2}{3}a_{02}\right)}{Ra^*\cos\phi(1+\pi a_{02})-\pi^2[(1+A^2)^2]/A^2}\right]^2. \tag{15}$$

Substituting the basic solution (11)–(13) into the linearized equations of the perturbation gives the following set of equations:

$$\frac{1}{A^2}\frac{\partial u}{\partial x}+\frac{1}{B^2}\frac{\partial v}{\partial y}+\frac{\partial w}{\partial z}=0; \tag{16}$$

$$-\nabla\pi+Ra^*\,\boldsymbol{k}\theta-\boldsymbol{v}=0; \tag{17}$$

$$\frac{\partial\theta}{\partial t}-\left[\frac{1}{A^2}\frac{\partial^2\theta}{\partial x^2}+\frac{1}{B^2}\frac{\partial^2\theta}{\partial y^2}+\frac{\partial^2\theta}{\partial z^2}\right]+\frac{1}{A^2}\left[U_0\frac{\partial\theta}{\partial x}+u\frac{\partial T_0}{\partial x}\right]$$
$$+\frac{1}{B^2}\left[V_0\frac{\partial\theta}{\partial y}+v\frac{\partial T_0}{\partial y}\right]+w\frac{\partial T_0}{\partial z}+W_0\frac{\partial\theta}{\partial z}=0; \tag{18}$$

corresponding to the rewriting of (1)–(3) using an orthogonal reference system with differently distorted coordinates. θ, $\boldsymbol{v}$, π stand for the temperature, velocity and pressure perturbations respectively with $\boldsymbol{v}=u\boldsymbol{e}_1+v\boldsymbol{e}_2+w\boldsymbol{e}_3$.

The transition we are searching for corresponds to the change from a unicellular regime to longitudinal coils. In this case the perturbations are taken as two-dimensional and then the horizontal component of the velocity perturbation is equal to zero ($u=0$).

The solution of the eigenvalue problem is carried out by adopting the following forms:

$$\theta=\cos m\pi y\sum_{k=1}^{N}A_k\sin k\pi z; \tag{19}$$

$$v=-Ra^*\pi^2B^2m\sin m\pi y\sum_{k=1}^{N}kB_k\cos k\pi z; \tag{20}$$

$$w=Ra^*\pi^2m^2\cos m\pi y\sum_{k=1}^{N}B_k\sin k\pi z; \tag{21}$$

where A_k and B_k, coefficients which are indeterminate using linear theory, are related by:

$$B_l=[\pi^2(B^2l^2+m^2)]^{-1}\cos\phi\,A_l=K_l\,A_l, \tag{22}$$

derived from the motion equation.

The solutions which satisfy the boundary conditions are:

$$\left.\begin{aligned} &v=0 \quad \text{in } y=0,\,1;\\ &w=0 \quad \text{in } z=0,\,1;\\ &\theta=0 \quad \text{in } z=0,\,1;\\ &\frac{\partial\theta}{\partial x}=\frac{\partial\theta}{\partial y}=0 \quad \text{in } x=y=0 \text{ and } x=y=1; \end{aligned}\right\} \tag{23}$$

and the continuity equation (16) leads to the following expression of the energy equation:

$$\frac{dA_l}{dt}=-\left(\frac{m^2}{B^2}+l^2\right)\pi^2A_l+Ra^*\pi^2m^2B_l-Ra^*\pi^3m^2a_{02}(B_{l+2}+B_{l-2}-B_{2-l}),$$

which can also be written, according to (22):

$$\frac{\mathrm{d}}{\mathrm{d}t}\left(\frac{B_l}{K_l}\right) = QB_l.$$

If the marginal state is defined by $\det Q = 0$ at the second order, an explicit instability criterion of flow is obtained:

$$Ra^* \cos\phi = \frac{\pi^2}{1+a_{02}\pi}\left(\frac{m}{B}+\frac{B}{m}\right)^2. \tag{24}$$

The a_{02} value characterizing the basic flow referring to pure conduction is given by:

$$8\pi^5 a_{02}(1+\pi a_{02})\left[Ra_0^* - \frac{\pi^2(1+A^2)^2}{A^2}\right]^2 + (16A\tan\phi\, Ra_0^2)\left(1+\frac{1}{A^2}\right)(1+\tfrac{2}{3}\pi a_{02})^2 = 0,$$

with

$$Ra_0^* = \pi^2\left(1+\frac{m^2}{B^2}\right)\left(1+\frac{B^2}{m^2}\right).$$

It can be shown that the a_{02} coefficient varies between 0 and $1/\pi$ and when the aspect ratio A tends to infinity a_{02} approaches zero. Therefore we can find again the classical criterion of stability:

$$Ra^* \cos\phi = 4\pi^2.$$

The results of the work done on stability are shown in figure 2 for different values of A. It can be observed that, with a given angle, the critical Rayleigh number is always greater than $Ra^* \cos\phi = 4\pi^2$, corresponding to an $(A \to \infty)$ infinite aspect ratio. This result emphasizes the stabilizing role of the confinement effect which enhances the unicellular flow in agreement with what has been shown by Jaffrennou and Bories (1974).

3.3. *Stability of the reversed flow*

When the porous layer is slightly inclined with respect to the horizontal line, the flow which takes place spontaneously is of unicellular type, rotating in the positive direction (upward current along the lower hot surface and downward current along the upper cold surface. If the Rayleigh number is lower than the critical value, which corresponds to the setting up of longitudinal rolls, the flow remains steady for the whole range of variation of the angle of inclination.

The two-dimensional numerical studies, of Walch & Dulieu (1981) and Caltagirone (1981), which enable a solution to be presented which corresponds to an inverse unicellular flow, characterized by a circulation in the negative direction, could exist in a porous cavity with aspect ratio $A = 1$. The conditions for the existence of this solution have been examined in a general case for some values of A greater than 1.

The algebraic equation which enables us to study the stability conditions on this flow, is a cubic equation, where the a_{11} coefficient is a variable, which represents the amplitude of the unicellular convective roll. Deduced from the three expressions (14) which give the relations between a_{02}, a_{11}, b_{11}, this equation is written as follows:

$$\begin{aligned} a_{11}^3 &\left\{\tfrac{1}{8}\pi^2 Ra^{*2}\cos^2\phi + Ra^{*2}\sin^2\phi\,\frac{16A^2}{9\pi^2}\left(1+\frac{1}{A^2}\right)\right\} \\ &+ a_{11}^2\left\{\tfrac{4}{3}A\,Ra^{*2}\sin\phi\cos\phi - Ra^*\sin\phi\,\frac{8\pi A}{3}\,\frac{(1+A^2)^2}{A^2}\right\} \\ &+ a_{11}\left\{-Ra^*\cos\phi\pi^2(1+A^2) - Ra^{*2}\sin^2\phi\,\frac{160A^2}{3\pi^4} + \frac{\pi^4(1+A^2)^3}{A^2}\right\} \\ &+ Ra^*\sin\phi\,\frac{16A(1+A^2)}{\pi} = 0. \end{aligned} \tag{25}$$

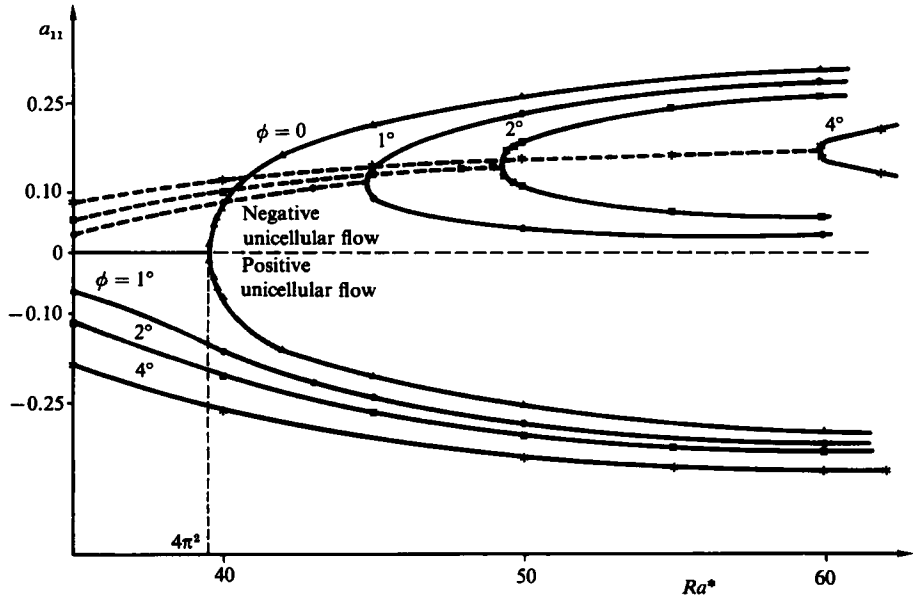

FIGURE 4. Amplitude of the a_{11} mode as a function of the Rayleigh number for several values of the angle ϕ and $A = 1$.

Where the aspect ratio is equal to 1 and ϕ to zero, we obtain:

$$a_{11}^2 = \frac{16(Ra^* - 4\pi^2)}{Ra^{*2}}, \tag{26}$$

which is illustrated in figure 4 by the existence of a roll which is able to rotate symmetrically in either direction from the bifurcation point $Ra^* = 4\pi^2$.

Three real solutions exist for the same value of the aspect ratio and for small angles: a solution corresponding to a positive unicellular flow and two solutions corresponding to a unicellular flow the direction of circulation one of which is the reverse of the preceding one. When the angle ϕ increases, the transition point (figure 4) at which these reverse solutions appears, is shifted towards large values of the Rayleigh number; when the angle of inclination is greater than about 6°, there is no longer a possibility of this flow existing.

All of these results have been confirmed by two-dimensional numerical computations (§4) which have demonstrated in particular that the value of the a_{11} coefficient found in this case was very close to the one calculated from the algebraic equation (25).

The influence of the extension A is, as observed for ϕ, a shifting of the transition point which corresponds to the existence of reversed solutions, towards large values of the Rayleigh number. As can be seen in figure 5 at $A = 2$, this result implies that the reverse flow can no longer exist when A increases.

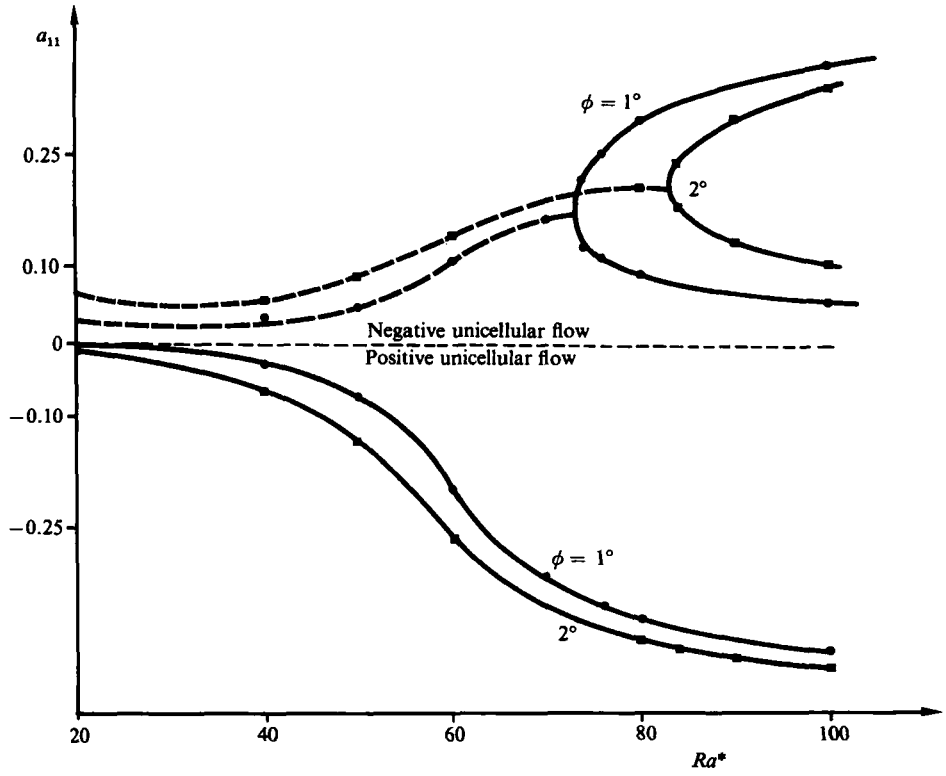

FIGURE 5. Amplitude of the a_{11} mode as a function of the Rayleigh number for several values of the angle ϕ and $A = 2$.

4. Two- and three-dimensional solutions

4.1. *The general numerical procedure*

The set of equations (1)–(3) has been solved numerically using a spectral method, the Galerkin mathematically based method, the setting up of which has been presented in a general case by Gottlieb and Orszag (1977). Expressions are developed for the temperature and the three velocity components using the following trial functions:

$$T = (1-z) + \sum_{l=0}^{L} \sum_{m=0}^{M} \sum_{n=0}^{N} a_{lmn}(t) \cos l\pi x \cos m\pi y \sin n\pi z; \tag{27}$$

$$U = -A^2 \sum_{l=1}^{L} \sum_{m=0}^{M} \sum_{n=1}^{N} b_{lmn} \ln \pi^2 \sin l\pi x \cos m\pi y \cos n\pi z; \tag{28}$$

$$V = B^2 \sum_{l=0}^{L} \sum_{m=0}^{M} \sum_{n=1}^{N} b_{lmn}\, mn\pi^2 \cos l\pi x \sin m\pi y \cos n\pi z; \tag{29}$$

$$W = \sum_{l=0}^{L} \sum_{m=0}^{M} \sum_{n=1}^{N} b_{lmn} (l^2+m^2) \pi^2 \cos l\pi x \cos m\pi y \sin \pi z. \tag{30}$$

These satisfy the boundary conditions given in figure 1 as well as the continuity equation (1). The method consists of finding the remainder by means of trial functions

and integrating over the whole volume. The pressure terms are eliminated by applying the divergence theorem and by taking into account the continuity equation. The equation of motion (3) allows the determination of the explicit relationships between the b_{ijk} and a_{ijk} coefficients:

$$b_{ijk} = Ra^* \cos\phi \frac{(i^2+j^2)}{(A^2i^2k^2+B^2j^2k^2+(i^2+j^2)^2)} a_{ijk} - Ra^* \sin\phi \frac{16A}{(A^2k^2+i^2)\, i^2k\pi^5} \delta_{i,2p-1}\delta_{k,2p-1} - Ra^* \sin\phi \sum_{l=0}^{L}\sum_{n=1}^{N} a_{ljn} \frac{16Ai^2kn\delta_{l-i,2p-1}\delta_{k-n,2p-1}}{(A^2i^2k^2+B^2j^2k^2+(i^2+j^2)^2)\,(l^2-i^2)\,(k^2-n^2)\,\pi^4}, \quad (31)$$

where $\delta_{i,2p-1} = 1$ if i is odd and $\delta_{i,2p-1} = 0$ if i is even.

If (27)–(30) are introduced into the energy equation, the following differential system is obtained:

$$\frac{da_{ijk}}{dt} = -\left(\frac{i^2}{A^2}+\frac{j^2}{B^2}+k^2\right)\pi^2 a_{ijk} + (i^2+j^2)\,\pi^2 b_{ijk} - \mathbb{N}(a, b), \quad (32)$$

where $\mathbb{N}$ is a nonlinear operator corresponding to the convective term $V\cdot\nabla T$. The initial conditions are represented by the temperature coefficients $a_{ijk}(0)$.

The nonlinear term of this system which corresponds to $V\cdot\nabla T$ can be processed in different ways: either the convolution product is analytically calculated and introduced into the differential system or the $V\cdot\nabla T$ product is obtained in the physical plane by first calculating V separately and then by coming back to the spectral plane using an inverse transform. The use of the FFT (fast Fourier transforms) for the calculation of the nonlinear terms reduces the computing time by a factor that can rise up to two orders of magnitude at approximations of relatively high order. Whichever type of processing may be chosen a nonlinear differential system in the spectral plane has to be solved, in which unknowns are the a_{ijk} coefficients (Caltagirone, Meyer & Mojtabi 1981; Straus & Schubert 1979).

The temporal resolution of the system (32) is made either by a fourth-order (Runge–Kutta) integration method, or by a second-order method of Adams–Bashforth type; both methods are explicit and only converge for relatively small timesteps which partially depend on the number of equations to integrate. The initial conditions of the a_{ijk} coefficients correspond to the superposition of the temperature perturbation upon the pure conduction state $T_0 = 1-z$.

The transient term of the system (32) is eliminated when the Rayleigh number is relatively small ($Ra^* < 250$), since it is then obvious that the solution converges to a stationary state. The a_{ijk} coefficients are obtained by resolving the nonlinear algebraic system, using the Newton–Raphson method, and introducing as starting coefficients some obtained at a smaller approximation. It must be noted that this process induces the flow structure *a priori*.

The expressions (27)–(30) being limited, the problem is to choose the number of terms to calculate, and to define an accuracy on any arbitrary quantity, which can be the heat transfer characterized by the Nusselt number. The number of terms chosen for each expression depends on the Rayleigh number and the A and B aspect ratios for a given accuracy of the Nusselt number. The higher the Rayleigh number, the greater the number of terms used, taking into account that it is necessary to represent some eventual micro-rolls generating oscillations, or even turbulence.

The total heat transfer between the isothermal areas can be obtained from the temperature expression (27):

$$Nu^* = \int_0^1 \int_0^1 -\left.\frac{\partial T}{\partial z}\right|_{z=0} \mathrm{d}x\,\mathrm{d}y = 1 - \pi \sum_{k=1}^{N} k a_{00k}. \tag{33}$$

One of the advantages of the Galerkin method used in this paper is that it is characterized by a semi-analytical form where some of the coefficients of the expressions can recreate the thermal field. Eventually this can be easily introduced into the perturbation equations in order to study the stability problem.

The calculations have been computed on IBM 3033 and CRAY 1.

4.2. *Two-dimensional solutions*

The solution of the two-dimensional flow can be obtained by setting $m = 0$ in (27)–(30). The results of the two-dimensional model have been compared with those of a finite-difference model, based upon the alternating directions algorithms (ADI) and the 'odd–even reduction' method (Horne & Caltagirone 1980), which uses up to 65×65 grids. The results are very close and will be discussed below.

Where one is looking for a very accurate solution of the unicellular flow concerning relatively small angles and with very short computation times, the temperature and velocity fields can be expressed as a function of the slope angle or, correspondingly, the a_{ik} and b_{ik} coefficients can be expressed as follows:

$$a_{ik} = \sum_{s=1}^{S} a_{ik}^s \phi^s; \tag{34}$$

$$b_{ik} = \sum_{s=1}^{S} b_{ik}^s \phi^s. \tag{35}$$

Introduction of these expressions into the momentum equation, or into (31), provides the relation between the b_{ik}^s and a_{ik}^s, say:

$$\begin{aligned} b_{ik}^s = {} & \sum_{r=0}^{s-2} a_{ik}^{s-r} \frac{\delta_{r,2p}(-1)^q}{r!} \frac{i}{(A^2k^2+i^2)\,\pi} - \frac{\delta_{s,2p-1}}{s!}(-1)^{q+1} \frac{16A}{(A^2k^2+i^2)\,\pi^4 ik}\, \delta_{i,2p-1}\delta_{k,2p-1} \\ & - \sum_{r=1}^{s-1} \sum_{l} \sum_{n} a_{ln}^{s-r} \frac{\delta_{r,2p-1}}{r!}(-1)^{q+1} \frac{16Akin}{(A^2k^2+i^2)\,\pi^3(l^2-i^2)\,(k^2-n^2)}\, \delta_{k-n,2p-1}\delta_{l-i,2p-1}. \end{aligned} \tag{36}$$

Substitution of (34)–(35) and the expression for b_{ik}^s into the energy equation (32) gives:

$$\begin{aligned} & -\left[Ra^* \frac{i^2}{(A^2k^2+i^2)} - \left(\frac{i^2}{A^2}+k^2\right)\pi^2\right] a_{ik}^s \\ & \quad = -\frac{\delta_{s,2p-1}(-1)^{q+1}}{s!} \frac{16A}{(A^2k^2+i^2)\,\pi^3 k}\, \delta_{i,2p-1}\delta_{k,2p-1} + \frac{i^2}{(A^2k^2+i^2)} \\ & \qquad \times \sum_{r=2}^{s-2} a_{ik}^{s-r} \frac{\delta_{r,2p-1}(-1)^q}{r!} - \frac{16i^2kA}{(A^2k^2+i^2)\,\pi^2} \sum_{r=1}^{s-1} \sum_{l=0}^{L} \sum_{n=1}^{N} a_{ln}^{s-r} \frac{\delta_{r,2p-1}(-1)^{q+1}}{r!} \\ & \qquad \times \frac{n}{(l^2-i^2)\,(k^2-n^2)} \delta_{l-i,2p-1}\delta_{k-n,2p-1} - Ra^* \frac{\pi^2}{4} \sum_{r=1}^{s-1} \sum_{l=0}^{L} \sum_{n=1}^{N} a_{ln}^{s-r} f(b^r), \end{aligned} \tag{37}$$

where the last term corresponds to the nonlinear term relating to the convective transport.

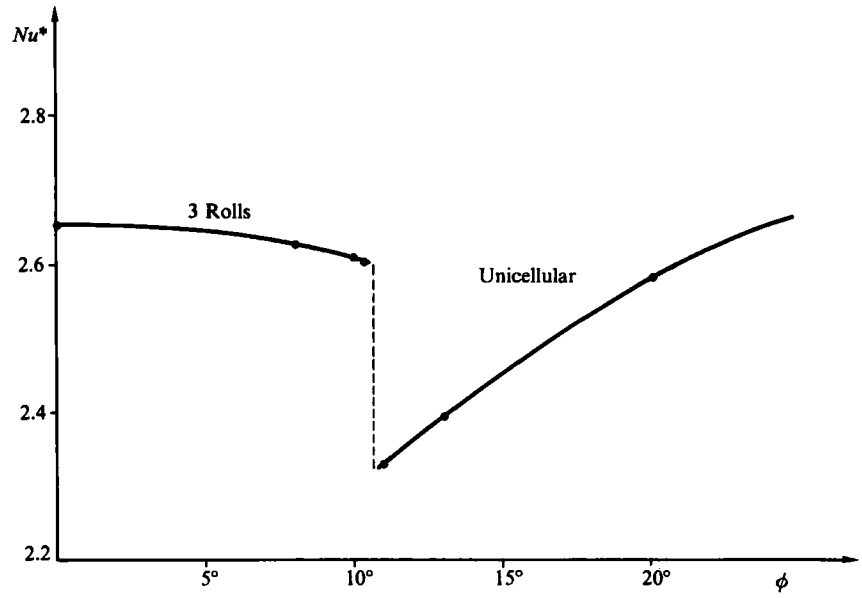

FIGURE 6. Variation of Nusselt number as a function of the angle for $Ra^* = 100$, $A = 2$.

The first term a^1_{ik} can be easily calculated:

$$a^1_{ik} = \left[Ra^* - \left(\frac{i}{A} + k^2 \frac{A}{i}\right)^2 \pi^2\right]^{-1} \frac{16A}{\pi^3 i^2 k} \delta_{i,2p-1} \delta_{k,2p-1}.$$

The successive coefficients of the series are then calculated from (37). This explicit procedure can be easily programmed and needs a very short computing time (Walker & Homsy 1978). Once the a^s_{ik} coefficients are known, they can be used to recreate the temperature field, to computer b^s_{ik} and then to obtain the velocity field $V = U(x, z)\, e_1 + W(x, z)\, e_3$. The expression rapidly converges at angles of inclination ϕ less than 20° for which the Nusselt number is within 1 % of the value given by the classical modelling.

5. Results

5.1. *Results of the two-dimensional modelling*

The calculations, which have been made in parallel using numerical models based either on the Galerkin method or on the finite-difference method, give approximately the same results when the number of degrees of freedom is great enough. The two-dimensional calculations are done in the following way: an arbitrary temperature distribution is given as the initial condition of the evolutive problem. This one is written as follows:

$$T = (1-z) + \alpha \cos(\beta \pi x) \sin \pi z,$$

where α and β are coefficients, α generally having a value of 0.05 or 0.1 and β being greater than the cell aspect ratio. This condition allows initiation of β convective rolls in the layer, some of them being damped out with time.

Figure 6 shows the evolution of the Nusselt number as a function of the ϕ slope at a Rayleigh number $Ra^* = 100$ and an aspect ratio $A = 2$. For small angles, the calculation leads to a stationary state consisting of three contra-rotating cells. Both

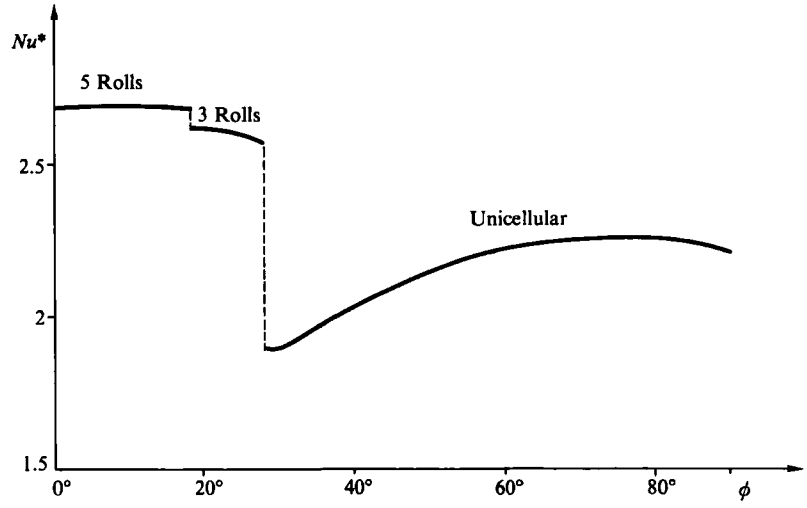

FIGURE 7. Variation of Nusselt number as a function of the angle for $Ra^* = 100$, $A = 4$.

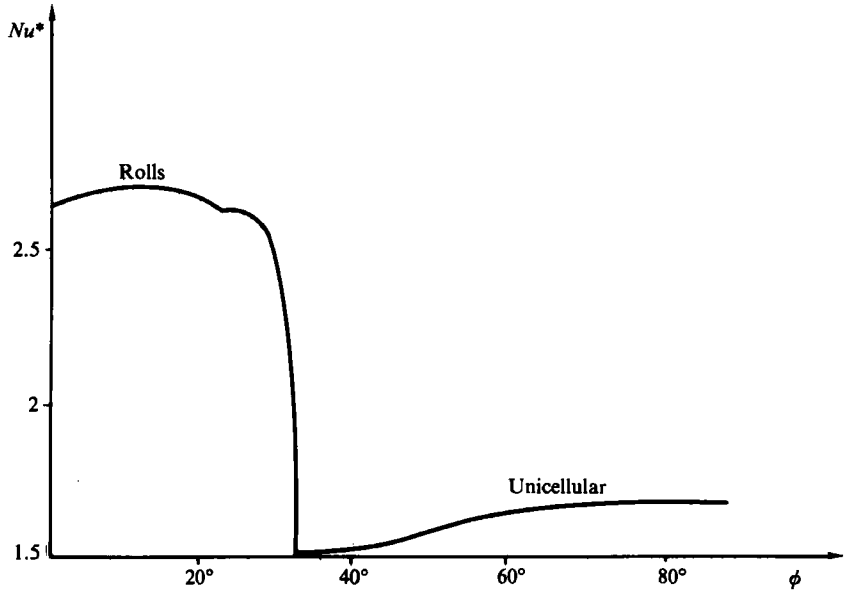

FIGURE 8. Variation of Nusselt number as a function of the angle for $Ra^* = 100$, $A = 8$.

of the outer cells rotate in positive directions. When the angle ϕ increases, the Nusselt number slightly decreases, and a sudden transition appears at an angle ranging between 10° 6′ and 11°. At this ϕ value, the flow becomes unicellular and the Nusselt number greatly decreases. If the angle ϕ continues to increase, the flow remains unicellular and the Nusselt number increases to $\phi = 90°$.

At a similar value of the Rayleigh number, $Ra^* = 100$, but, with $A = 4$, the same phenomenon occurs (figure 7) and five-cell, then three-cell, and finally unicellular, flows evolve as the slope increases. It will be noted that, in this case, the transition between the tricellular and the unicellular flow is obtained at 28° instead of 10° 8′

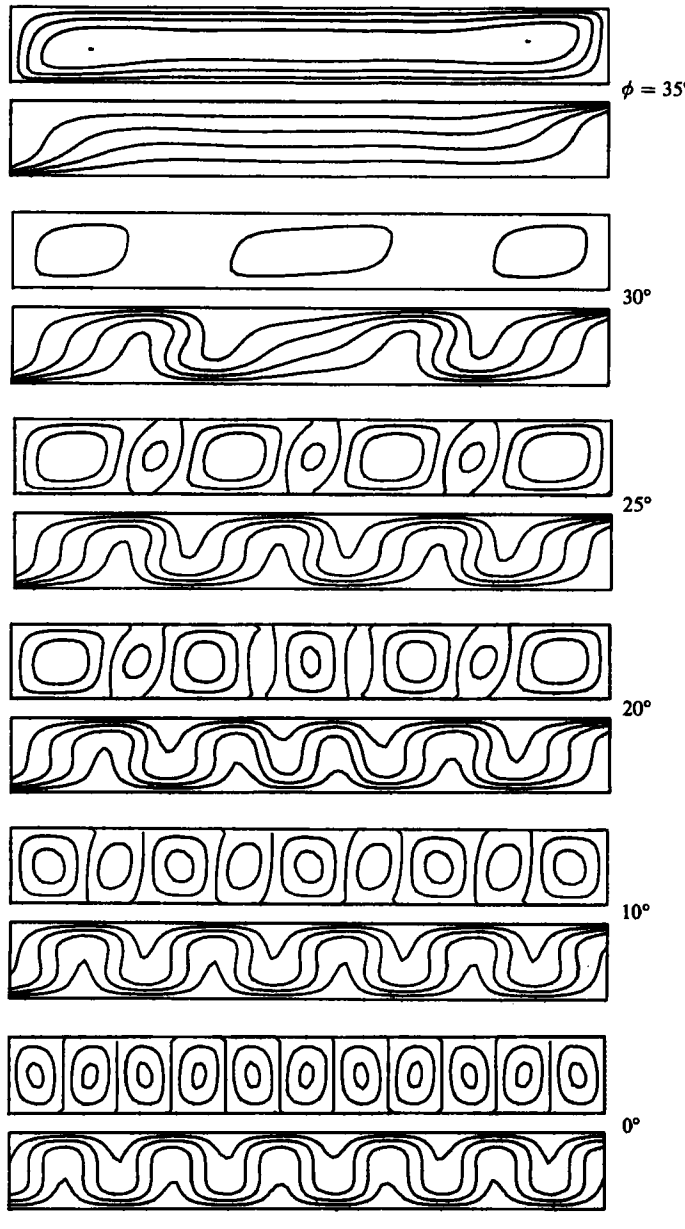

FIGURE 9. Isotherms and streamlines for various ϕ values, $Ra^* = 100$, $A = 8$.

for $A = 2$, and that during this transition the Nusselt number decreases sharply from 2.6 to 1.9 before increasing slowly.

Keeping the Rayleigh number equal to 100, calculations for $A = 8$ show the flow transitions passing from nine, to seven, then five cells before degenerating into a single cell at an angle ϕ, varying from 30° to 32°. The temperature field and the streamlines associated with this series of transitions are represented in figure 9 and the corresponding evolution of the Nusselt number in figure 8.

To summarize, the results for two-dimensional convection in an inclined porous

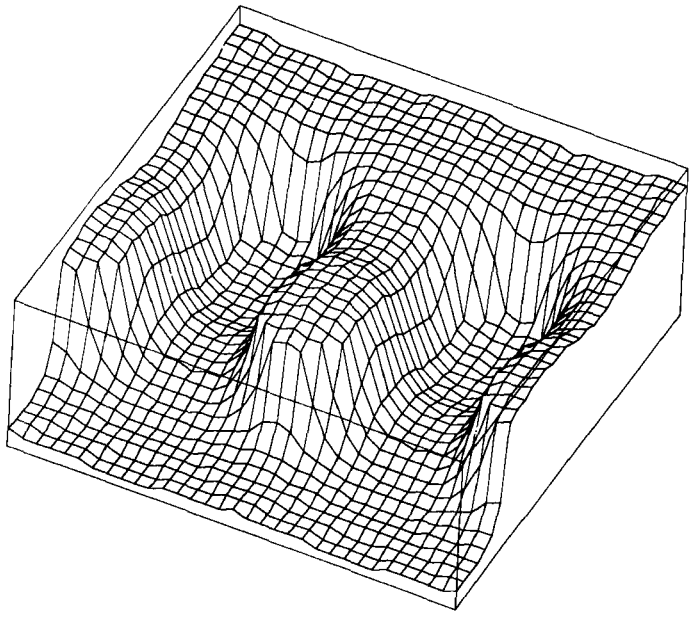

FIGURE 10. Isotherm $T = 0.5$ for $A = 3$, $B = 3$, $Ra^* = 100$, $\phi = 20°$. Initial conditions are longitudinal coils.

layer enable us to illustrate the different transitions which explain the number of rolls decreasing at odd values when the angle ϕ increases, and also to find the critical value of the slope ϕ_t corresponding to the change of the flow from transverse rolls to unicellular flow. Depending on the aspect ratio A, this value tends rapidly towards 31° for large aspect ratios, the values corresponding well with the results obtained from the linear analysis of the unicellular flow stability, $\phi_t = 31° 48'$, presented in §3.

This excellent correlation is due largely to the fact that the flow outside the immediate vicinity of the ends tends rapidly towards the analytical solution U_0 introduced in the perturbation equations. As mentioned by Jaffrennou and Bories (1974), we have observed that, when the aspect ratio of the layer decreases, the effect of the longitudinal confinement can be described by the mean value of the temperature gradient along this axis.

5.2. *Results of the three-dimensional modelling*

The numerical modelling presented in §4.1 enables us to get some results concerning the flow configurations that can be developed in porous layers having respectively the parameters ($A = 3$, $B = 3$), ($A = 6$, $B = 4$), and ($A = 8$, $B = 4$). The value of the Rayleigh number, $Ra^* = 100$, has been chosen in order to observe well-developed but stationary flows. The results obtained allow us to confirm:

(i) the existence of a unicellular flow when the angle of inclination is close to 90°. This flow is established, for the three sets of parameters considered, as the initial temperature field corresponding to a pure-conduction situation is perturbed by a white noise ($a_{ijk}(0) = 10^{-3}$);

(ii) the existence of a flow with longitudinal coils. Whatever the type of initial conditions imposed, this flow naturally evolves during the period when the value of the angle of inclination is effectively included in domain III of the stability diagram (figure 2);

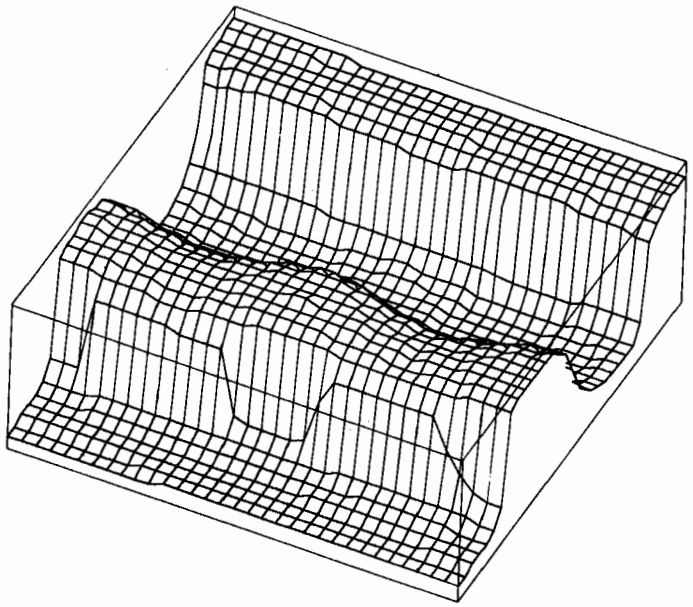

FIGURE 11. Isotherm $T = 0.5$ for $A = 3$, $B = 3$, $Ra^* = 100$, $\phi = 20°$. Initial conditions are transversal rolls.

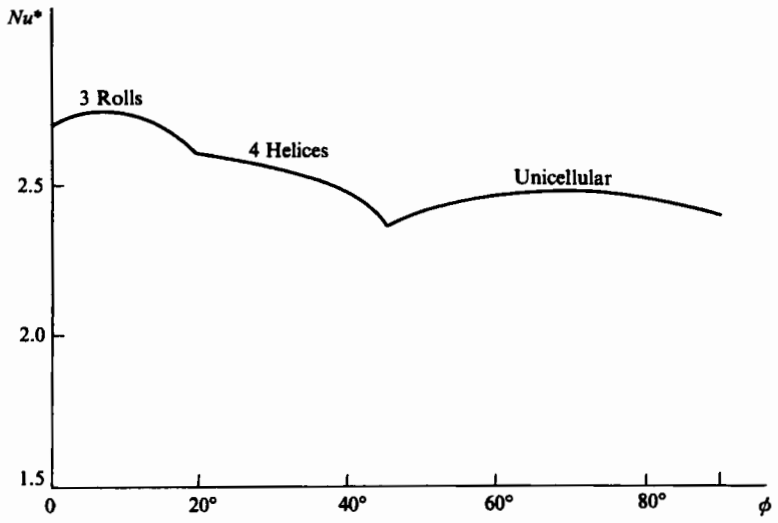

FIGURE 12. Variation of Nusselt number for various ϕ values, for $Ra^* = 100$, $A = 3$, $B = 3$.

(iii) the existence of more complex three-dimensional flow structures, mainly characterized by transverse rolls or by the superposition of transverse and longitudinal rolls, for slope angles included in domain II in figure 2.

It is worth noting, however, that for the latter values of the slope (domain II) it was observed that the final configuration was largely dependent on the temperature field which was given as an initial condition by means of the a_{ijk} modes. This is particularly true for the cavity with parameters ($A = 3$, $B = 3$), in which it was verified that several induced three-dimensional structures, characterized by the a_{ijk} modes, do converge to a stable solution of this type.

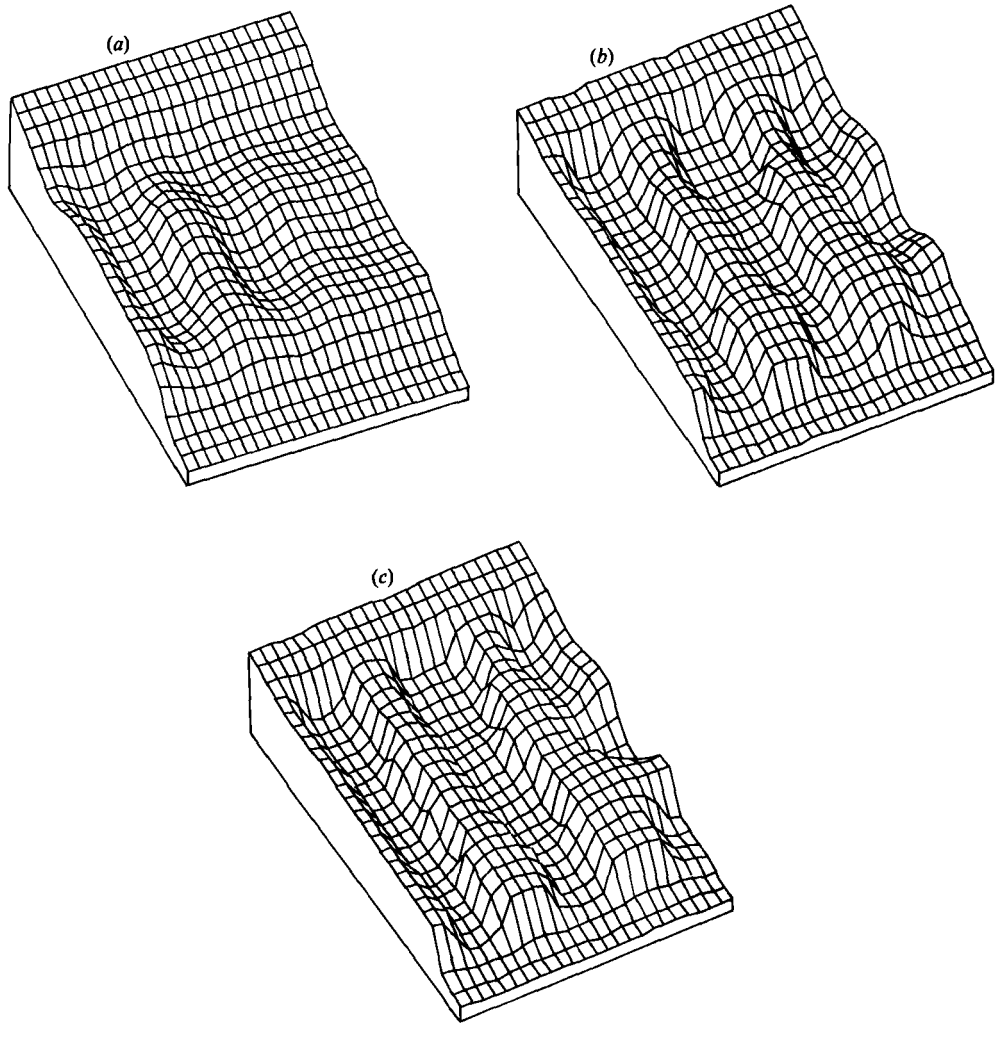

FIGURE 13. Evolution of the isotherm $T = 0.5$ over time, for $A = 6$, $B = 4$, $Ra^* = 100$, $\phi = 30°$.

All these results, which essentially correspond to the theoretical predictions and the previous experimental observations (Bories & Combarnous 1973), are illustrated (by examples) in figures 10–14.

Figures 10 and 11 show flow configurations with mainly transverse and longitudinal rolls, the visualization of these flows being given by the drawing of the isotherm 0.5. Figure 12 shows the evolution of the Nusselt number corresponding to these flows, up to the presence of the unicellular flow rate, as a function of the slope.

Figures 13(*a*)–(*c*) follow through a calculation for a white noise at a Rayleigh number of 100 and slope angle of 30°. It will be noted that the perturbation of longitudinal rolls amplifies from the abscissa, $y = 0$, on an already developed unicellular flow, reaches the opposite side, $y = 1$, and becomes connected there with the aid of the transverse rolls. The last figure, 13(*c*), shows the stationary regime where the transverse structure persists across a small part of the layer.

In figure 14 the influence of the initial conditions are illustrated, showing how a

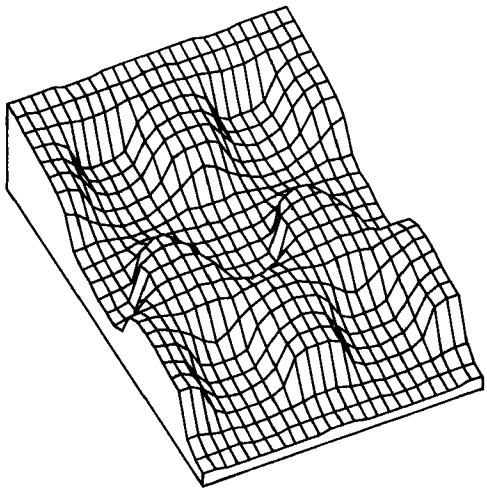

FIGURE 14. Isotherm $T = 0.5$ for $A = 6$, $B = 4$, $Ra^* = 100$, $\phi = 30°$.

ϕ	Nu^*	Initial condition	Final flow
0	2.677	$a(0, 5, 1)+a(9, 0, 1)$	$a(9, 0, 1)$
10	2.687	$a(13, 7, 1) = -0.1$	$a(9, 0, 1)$
10	2.695	$a(0, 5, 1)+a(9, 0, 1)$	$a(9, 0, 1)$
20	2.580	$a(0, 4, 1) = -0.1$	$a(0, 4, 1)$
20	2.583	$a(0, 5, 1)+a(9, 0, 1)$	$a(0, 5, 1)$
20	2.617	$a(7, 0, 1) = -0.1$	$a(7, 0, 1)$
20	2.653	$a(13, 7, 1) = -0.1$	$a(9, 0, 1)$
30	2.473	$a(0, 5, 1)+a(9, 0, 1)$	$a(5, 0, 1)$
45	2.169	$a(0, 5, 1)+a(9, 0, 1)$	$a(0, 5, 1)$
60	1.562	$a(13, 7, 1) = -0.1$	$a(0, 1, 1)+a(0, 3, 1)$ (unicellular)

TABLE 2. Three-dimensional inclined porous layer: $Ra^* = 100$; $A = 8$; $B = 4$

perturbation corresponding to the mode (6, 4, 1), which is used as an initial condition for the same angle $\phi = 30°$, develops and leads to a stationary state of the same type. This influence of the initial conditions on the various observed solutions is all the more important as the aspect ratios increase. Therefore, the calculations on CRAY 1, with $32 \times 16 \times 8$ modes, and considering the mode (13, 7, 1) as an initial condition, which corresponds to a superimposed transverse and longitudinal roll structure of either (0, 5, 1) or (0, 0, 1), lead to the results given in table 2, in which the initial conditions of the calculation and the final flow are mentioned.

As we can see, calculations do not allow us to predict the stationary state to which the flow induced by the given initial conditions converges, due to the large number of structures that can be found for a single configuration.

6. Conclusion

The numerical predictions presented in this paper support the theoretical analysis and interpretation of the experimental observations previously done by Bories & Monferran (1972), Bories & Combarnous (1973), Jaffrennou & Bories (1974) and

Walch & Dulieu (1979) on the natural convection in an inclined porous layer. Many of the results correspond exactly with those previously obtained: the existence of three major flow domains, in the (Ra^*, ϕ)-plane; the stabilizing influence of the longitudinal confinement on the basic unicellular flow; and the value of the stability criterion of the unicellular flow, equal to $Ra^* \cos\phi \leqslant 4\pi^2$ and $A \to \infty$. In addition this study introduces new elements in several areas, particularly:

(i) the existence of a transition slope ϕ_t, characterizing the change of the flow domain into polyhedric cells (domain I), or the flow domain of longitudinal rolls (domain II),

(ii) the determining role of the initial conditions in the selection of stationary modes when ϕ is less than ϕ_t.

Limited to and calculated for an infinite extension layer in a three-dimensional case, the theoretical value $\phi_t = 31°\,48'$ always differs quite noticeably from the first experimental estimations, $\phi_{t\text{exp}} \approx 15°$. The source of the disagreement (which can be initially imputed to the influence of the extension A) is currently being investigated by further experimental and numerical studies.

The authors would like to thank the 'Centre de Calcul Vectoriel pour la Recherche' and the 'Centre Notional Universitaire Sud de Calcul' for their support and the time they provided us for computation.

REFERENCES

Bories, S. & Combarnous, M. 1973 Natural convection in a sloping porous layer. *J. Fluid Mech.* **57**, 63–79.

Bories, S., Combarnous, M. & Jaffrenou, J. Y. 1972 Observations des differentes formes d'ecoulements thermoconvectifs dans une couche poreuse inclinée. *C.R. Acad. Sci. Paris* A **275**, 857–860.

Bories, S. & Monferran, L. 1972 Condition de stabilité et échange thermique par convection naturelle dans une couche poreuse inclinée de grande extension. *C.R. Acad. Sci. Paris* B **274**, 4–7.

Caltagirone, J. P. 1975 Thermoconvective instabilities in a porous layer. *J. Fluid. Mech.* **72**, 269–287.

Caltagirone, J. P. 1981 Convection in porous medium. In *Convective Transport and Instability Phenomena*, (ed. G. Braun) pp. 199–232, Karlsruhe.

Caltagirone, J. P. & Bories, S. 1980 Solutions numériques bidimensionnelles et tridimensionnelles de l'écoulement de convection naturelle dans une couche poreuse inclinée. *C.R. Acad. Sci. Paris* B **190**, 197–200.

Caltagirone, J. P., Meyer, G. & Mojtabi, A. 1981 Structurations thermoconvectives tridimensionnelles dans une couche poreuse horizontale. *J. Méc.* **20**, 219–232.

Chan, B. K. C., Ivey, C. M. & Barry, J. M. 1970 Natural convection in inclosed porous media with rectangular boundaries. *Trans. ASME* C: *J. Heat Transfer* **92**, 21–27.

Combarnous, M. & Bories, S. 1975 Hydrothermal convection in saturated porous media. *Adv. Hydrosci.* **10**, 231–307.

Gottlieb, P. & Orszag, S. A. 1977 *Numerical Analysis of Spectral Methods, Theory and Applications*. Regional Conf. Series in Applied Maths, vol. 26. Arrowsmith.

Horne, R. N. 1979 Three-dimensional natural convection in a confined porous medium heated from below. *J. Fluid Mech.* **92**, 751–766.

Horne, R. N. & Caltagirone, J. P. 1980 On the evolution of thermal disturbances during natural convection in a porous medium. *J. Fluid Mech.* **100**, 385–395.

Jaffrennou, J. Y. & Bories, S. 1974 Convection naturelle dans une couche poreuse inclinée. *Rapport interne G.E.* 14. Institut de Mecanique des Fluides de Toulouse.

SCHUBERT, G. E. & STRAUS, J. M. 1979 Three-dimensional and multicellular steady and unsteady convection in fluid-saturated porous media at high Rayleigh numbers. *J. Fluid Mech.* **94**, 25–38.

STRAUS, J. M. & SCHUBERT, G. E. 1979 Three-dimensional convection in a cubic box of a fluid-saturated porous material. *J. Fluid Mech.* **91**, 155–165.

WALCH, J. P. 1980 Convection naturelle dans une boîte poreuse inclinée: contribution à l'étude du cas stable. Thèse Université Paris VI.

WALCH, J. P. & DULIEU, B. 1979 Convection naturelle dans une boîte rectangulaire légèrement inclinée contenant un milieu poreux. *Intl J. Heat Mass Transfer* **22**, 1607–1612.

WALCH, J. P. & DULIEU, B. 1982 Convection de Rayleigh–Bénard dans une cavité poreuse faiblement inclinée. *Journal de Physiques Lettres.* **43**, L103–107.

WALKER, K. L. & HOMSY, G. M. 1978 Convection in a porous cavity. *J. Fluid Mech.* **87**, 449–474.

WEBER, J. E. 1975 Thermal convection in a tilted porous layer. *Intl J. Heat Mass Transf.* **18**, 474–475.